Journal of Zhejiang University-SCIENCE A (Applied Physics & Engineering) 2022 23(10):783-794
www.jzus.zju.edu.cn; www.springer.com/journal/11582
E-mail: jzus_a@zju.edu.cn

Research Article

https://doi.org/10.1631/jzus.A2200159

Effect of droplet superficial velocity on mixing efficiency in a microchannel

Jin-yuan QIAN[1,2], Lei ZHAO[1], Xiao-juan LI[1], Wen-qing LI[1], Zhi-jiang JIN[1]✉

[1]*Institute of Process Equipment, College of Energy Engineering, Zhejiang University, Hangzhou 310027, China*
[2]*State Key Laboratory of Fluid Power and Mechatronic Systems, Zhejiang University, Hangzhou 310027, China*

Abstract: In this study, droplet characteristics including droplet length and formation time, and mixing efficiency in droplets were investigated via the volume of fluid (VOF) method coupled with a user defined scalar (UDS) model. A cross-shaped junction with a square cross-section was designed and used for droplet formation. An initial arrangement which differed from that of a conventional operation was adopted. Results show that when the droplet superficial velocity is constant, the exchange between the dispersed phase velocity and the continuous phase velocity has a marginal effect on the droplet formation time. However, the exchange has a great effect on droplet length. These findings provide a valuable guide for future operation of droplet formation. In addition, the results show that the mixing efficiency in the droplet forming stage can be classified into time-dominated and length-dominated regimes according to the droplet superficial velocity. When a droplet flows in a microchannel, a higher droplet superficial velocity increases mixing efficiency due to the faster inner circulation and shorter droplet length.

Key words: Droplet characteristics; Mixing efficiency; Inner circulation; Droplet superficial velocity

1 Introduction

Microfluidic systems are increasingly being used in organic syntheses, drug delivery, and food processing (Mu et al., 2019; Cao et al., 2020; Mehta and Rath, 2021; Niculescu et al., 2021; Zhang et al., 2021) due to their superior performance compared with traditional equipment. Mixing and mass transfer are very important processes in microfluidic systems. The droplet-based method, in which the fluid mixing or the mass transfer between phases is limited in a droplet, has proved to be an effective way to enhance mixing and mass transfer processes (Luo et al., 2019; Liu et al., 2021). When the droplet is flowing through the microchannel, the interactions between the droplet and the channel wall, and between the droplet and the continuous phase induce an inner circulation in the droplet and reduce the thickness of the boundary layer between the phases. They both facilitate the performance of the mixing and mass transfer (Özkan and Erdem, 2015; Zhang et al., 2015).

Studies of the mass transfer between phases are dominated by experimentation, mostly involving chemical reactions. Neutralization of an acid with alkali is widely used. Alkali and acid are added as aqueous phase and organic phase, respectively. With the droplet moving, the acid transfers from the organic phase into the aqueous phase and reaction happens (Yeh et al., 2015; Sattari-Najafabadi et al., 2017). Indicators such as bromothymol blue, phenol red, and Sudan III are added in the aqueous phase or organic phase. When mass transfer between phases occurs without reactions, extraction is more often used (Hosseini Kakavandi et al., 2016; Dai et al., 2017). The reaction process is visualized by the color change of the phases which include indicators. The mass transfer efficiency is quantified by the overall mass transfer coefficient, which is based on the timing of the color change of the indicator and the concentration of the acid (alkali) (Tsaoulidis and Angeli, 2015; Zhang et al., 2019).

However, simulation methods are more commonly used to investigate the mixing process in a

✉ Zhi-jiang JIN, jzj@zju.edu.cn
Jin-yuan QIAN, https://orcid.org/0000-0002-5438-0833
Zhi-jiang JIN, https://orcid.org/0000-0002-8063-709X

Received Mar. 24, 2022; Revision accepted June 29, 2022;
Crosschecked Aug. 29, 2022

droplet. In a numerical simulation, scalars are added in the partially dispersed phase, so the dispersed phase contains two parts: the dispersed phase with scalars and the dispersed phase without scalars. The mixing process in the droplet is visualized by the distribution of scalars, and quantified by calculating the scalar concentration in the specified droplet. That is, scalars in numerical simulations are equivalent to indicators in experiments. The mixing process in the droplet can be divided into two stages depending on the initial distribution of the scalars. One of the earliest investigations considering the distributions of the mixing components was carried out (Tanthapanichakoon et al., 2006). Distributions of the mixing components in the droplet were considered as two types: a front/back distribution and a lower/upper distribution. In the droplet forming stage, the dispersed phase flows through the microchannel and interacts with the continuous phase. Shearing interactions between the two phases disturb the velocity fields located in the tip of the forming droplet, and induce an eddy. The formation of the eddy was described as "twirling" (Tice et al., 2003). Scalar transforms from the higher concentration to the lower concentration due to the twirling effect. Thus, when the mixing components are distributed initially in the front/back parts of the droplet, the mixing efficiency can be greatly enhanced during the droplet forming stage. The overall mass transfer coefficients in both the droplet forming stage and droplet moving stage were calculated by investigating the mass transfer behaviors of Rhodamine 6G ($C_{28}H_{31}N_2O_3Cl$) from a water droplet to an ionic liquid (Bai et al., 2016). Results showed that the overall mass transfer coefficient in the droplet forming stage was three or four times higher than that in the droplet moving stage. When the mixing components are distributed initially in the lower/upper parts of the droplet, the mixing process is enhanced mainly during the droplet moving stage. The microchannels need to be designed with a more complex structure for disturbing the droplet (Bai et al., 2018; Borgohain et al., 2018; Fu et al., 2019; Qian et al., 2019b). When the droplet is moving through the microchannel, mixing performance is enhanced by introducing a serpentine with a different bend radius (Qian et al., 2019a). The mixing efficiency for different bend radii was quantified and the Dean numbers calculated to further explain the mixing performance caused by variation in the bend radius. Results showed that the turns greatly promoted the mixing efficiency. When the droplet was moving out of the first turn, the mixing efficiency was five times higher than that in the droplet forming stage. Approaches including the introductions of a T/Y-junction and a deforming microchannel were proposed to improve the mixing efficiency in droplets which formed in a simple cross-shaped microchannel (Bai et al., 2018). Comparisons indicated that the design of a Y-deforming microchannel had excellent performance for enhancing the mixing efficiency. Besides introducing a complex structure, micro-particle packing is an alternative way to enhance the mixing efficiency (Su et al., 2010). Whether the mixing components have a front/back distribution or a lower/upper distribution in the droplet size, the mixing efficiency is greatly affected by the droplet length. The twirling effect, which dominates in the droplet forming stage, is closely associated with the droplet length. For shorter or longer droplets, the mixing efficiency is worse due to an over-twirling effect or under-twirling effect. In addition, in the droplet moving stage, the symmetrical inner circulation in a larger droplet is more difficult to break than that of a smaller droplet. Results indicate that a suitable droplet length for fluid mixing is $L/w\approx1$, where L represents the droplet length and w represents the microchannel width (Wang et al., 2015; Bai et al., 2018; Qian et al., 2019c, 2021; Jin et al., 2020).

For a specified two-phase system, parameters including dispersed phase fraction, droplet superficial velocity, microchannel geometry, and operating conditions are of great importance for the mixing process in the droplet. The droplet superficial velocity is defined simply as the sum of the dispersed phase and the continuous phase. The dispersed phase fraction determines the velocity of the continuous phase and dispersed phase. By investigating the effect of the dispersed phase fraction on droplet formation and mixing in the droplet, it was found that the mixing performance declined with an increase of the dispersed phase fraction. The increased dispersed phase fraction led to an increase in droplet length (Madadelahi and Shamloo, 2017; Qian et al., 2019a). Therefore, more time was required to achieve an ideal mixing efficiency. Microchannel structures, including the dimensions of the microchannel, the junction structure, and the main channel structure, play an important role in the relocation of the mixing components. The mixing

performance of square cross-section microchannels is better than that of rectangular microchannels of the same hydraulic diameter (Sattari-Najafabadi et al., 2017). By studying the mixing performance in microchannels with a cross-shaped junction, cross-shaped T-junction, and T-junction, it was shown that when the dispersed phase fraction was in a lower range, a cross-shaped T-junction was more suitable for fluid mixing. With an increase of the dispersed phase fraction, superiority of the cross-shaped junction was more apparent (Qian et al., 2019a). A numerical method for the splitting process of two-phase flow in a multi-parallel branched microchannel was established, and the pressure variation and flow distribution of the microchannel under different splitting modes were analyzed. The results showed a strong two-way coupling effect between the outlet pressure and mass flow in the branch (Zhang et al., 2022).

The droplet superficial velocity is also an important parameter in determining the mixing performance in the droplet. Variation in the droplet superficial velocity affects the interface renewal frequency and overall transport time in microfluidic systems. The objective of this study was to present the effect of droplet superficial velocity on droplet characteristics, and then to study the relationship between mixing performance and droplet characteristics.

2 Computational model

2.1 Governing equations

Simulations were conducted in ANSYS Fluent 17.2. The volume of fluid (VOF) method was used for the transient tracking of the liquid-liquid interface. The interface tracking between the phases was solved by the solution of a continuity equation, as in Eq. (1).

$$\nabla \boldsymbol{v} = 0, \tag{1}$$

where $\boldsymbol{v}$ is the velocity vector. The density and viscosity of the studied two-phase in each computational cell were calculated using Eqs. (2) and (3), respectively.

$$\rho = \alpha_c \rho_c + \alpha_d \rho_d, \tag{2}$$

$$\mu = \alpha_c \mu_c + \alpha_d \mu_d, \tag{3}$$

where ρ denotes the density; μ represents fluid viscosity; α denotes the volume fraction; the subscripts c and d represent the continuous and dispersed phases, respectively.

In addition, a user-defined scalar (UDS) was defined and added to the dispersed phase for visualization of the mixing process (Wu et al., 2022). The transport equation for the scalars was

$$\frac{\partial \rho_d \phi}{\partial t} + \nabla \cdot (\rho_d \boldsymbol{v} \phi - \Gamma \cdot \nabla \phi) = 0, \tag{4}$$

where t is the time, ϕ represents the scalar, and Γ represents the diffusion coefficient. Detailed descriptions can be found in our previous publication (Qian et al., 2019a).

2.2 Geometrical model and boundary conditions

Fig. 1 shows a schematic diagram of a microchannel with a cross-shaped junction. The microchannel was designed with a square cross-section with the dimensions $w_c \times w_d \times h$=100 μm×100 μm×100 μm.

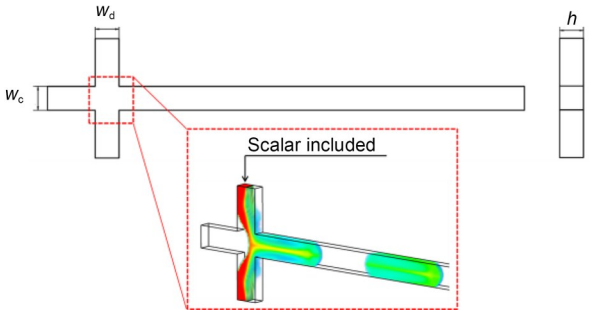

Fig. 1 Schematic diagram of the microchannel. References to color refer to the online version of this figure

The dispersed phase is injected through the vertical channel and the continuous phase through the horizontal channel. The properties of the two liquids were consistent with those in the experiment presented by Nisisako et al. (2004). Table 1 shows the physical

Table 1 Physical properties of the dispersed phase and the continuous phase

Parameter	Value
μ_d (Pa·s)	6.71×10^{-3}
ρ_d (kg/m^3)	1020
μ_c (Pa·s)	1.95×10^{-3}
ρ_c (kg/m^3)	1000
σ (mN/m)	33.5

properties of both phases. In Table 1, σ represents the surface tension. Each of the dispersed phase channels is divided into two equal parts. For the visualization of the mixing process, a scalar is added to half of the dispersed phase (Fig. 1) and marked with red color. Velocity inlet and outflow were set at the inlet and outlet, respectively.

2.3 Quantification of the mixing efficiency

Mixing efficiency in a droplet is represented by the uniformity of the scalar distribution. Fig. 1 shows that at the beginning of droplet formation, the scalar is distributed symmetrically in the dispersed phase. As the dispersed phase flows into the microchannel and interacts with the continuous phase, the scalar is relocated due to the disturbed velocity fields in the droplet. Eq. (5) was defined to quantify the mixing efficiency in the droplet.

$$\mathrm{ME}=\left(1-\frac{\sqrt{\frac{1}{N}\sum_{i=1}^{N}(c_i-\bar{c})^2}}{\bar{c}}\right)\times 100\%, \tag{5}$$

where ME represents the mixing efficiency, defined based on the standard deviation of the ideal condition; c_i is the arbitrary node concentration of the scalar; $\bar{c}$ is the ideal concentration; N is the number of nodes in a confined droplet size. When achieving an ideal condition, the scalar is distributed in the droplet uniformly and the scalar concentration in each node is 0.5.

2.4 Grid independence check

The mesh was generated via the pre-processor meshing in ANSYS Workbench 17.2. Fig. 2 shows the variation of the mixing efficiency with different mesh numbers. The mesh numbers were increased from No. 1 (80000) to No. 7 (500000). With increasing mesh numbers, the mixing efficiency decreased and then fluctuated within a limited range. When the mesh number was greater than 330000 (No. 5), the mixing efficiency was independent of the mesh number. Therefore, the mesh size corresponding to the mesh number of 330000 (No. 5) was selected to generate the mesh for the geometry. In addition, the droplet length for different mesh numbers was measured. Data showed that the droplet length fluctuated within only a small range. The relative error between the maximum and minimum values of the droplet length was less than 3%. Thus, the selected mesh size was sufficient for analysis of the droplet formation.

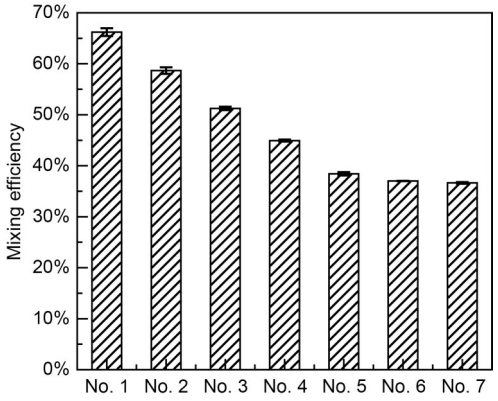

Fig. 2 Dependency of mixing efficiency on the mesh numbers

3 Validation of the simulation method

Observation of mixing in a droplet via a numerical approach is considered as a useful tool (Özkan and Erdem, 2015; Wang et al., 2015; Zhang et al., 2015; Fu et al., 2019). Our previous studies also testified to the effectiveness of numerical simulation. Experiments carried out previously (Tice et al., 2003; Oishi et al., 2009; Cao et al., 2018) were selected for the simulations, and the results compared with experimental data. Both the characteristics of the droplet and the mixing process in the droplet were considered. The hydraulic diameter and the phase properties used in the simulations were kept consistent with those used in the experiments. The droplet length was as measured and reported (Tice et al., 2003), and the droplet formation process was as presented in simulations and reported (Cao et al., 2018). The velocity fields illustrated by the simulations and recorded by particle image velocimetry (PIV) method (Oishi et al., 2009) showed high consistency. Fig. 3 shows comparisons between numerical simulation of the mixing process in the droplet with the experimental results (Tice et al., 2003) presented in our previous study (Qian et al., 2019b).

4 Results and discussion

In this section, we present results from analysis of the effect of droplet superficial velocity on droplet

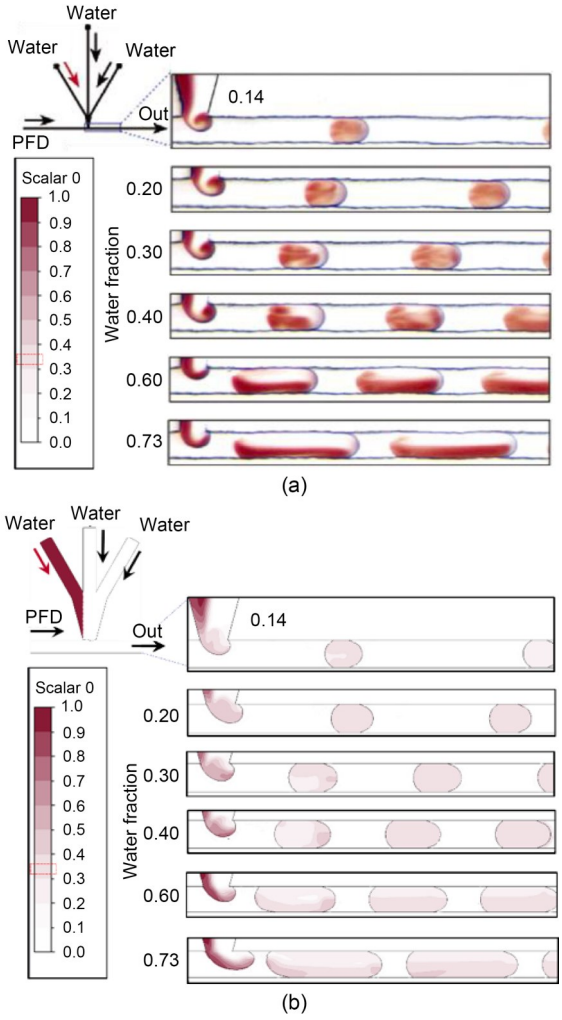

Fig. 3 Comparison of results from experimentation and simulation of the mixing process (Qian et al., 2019b): (a) experimental results; (b) simulation results. PFD represents the perfluorodecalin

formation and mixing in a droplet. The droplet superficial velocity varied from 10 to 100 mm/s. Velocities of the dispersed phase (u_d) and the continuous phase (u_c) were determined by the dispersed phase fraction, ε_d, and the droplet superficial velocity, u_{sup}, as shown in Eqs. (6) and (7).

$$u_d = \varepsilon_d u_{sup}, \tag{6}$$

$$u_c = u_{sup} - u_d. \tag{7}$$

4.1 Droplet formation process

Fig. 4 shows the droplet formation process in the simulations. The abscissa represents a complete droplet formation time t, and the ordinate represents pressure fluctuation during the droplet formation time. The droplet formation process included four stages: a lag stage (I), a blocking stage (II), a surface-renewal stage (III), and a squeezing stage (IV). Among the four stages, the blocking stage and squeezing stage were the most common. These two stages occurred regardless of the junction structure of the microchannel and the inlet distribution of the two phases. Whether the junction structure was a T-junction, Y-junction, cross-shaped junction, or any other, the blocking stage and squeezing stage invariably occurred in the droplet formation process (Korczyk et al., 2019; Qian et al., 2019b; Zhang et al., 2019). Occurrence of the lag stage depended on the microchannel dimensions, the velocity of the dispersed phase, and the viscosity of the dispersed phase. The lag stage increased the droplet formation time and counteracted the mass production of the droplet. When fabricating the T-junction microchannel, the dispersed phase channel width should be at least equal to half the continuous phase channel width to reduce the time spent in the lag stage (Qian et al., 2019b).

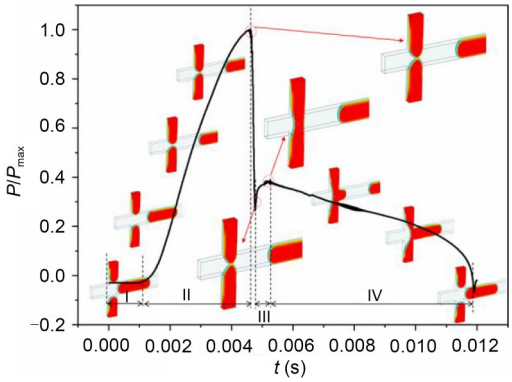

Fig. 4 Schematic diagram of droplet formation with u_{sup}= 50 mm/s and ε_d=0.5

The surface-renewal stage is a new phenomenon. Its occurrence depended on the inlet distribution of the two phases, especially in the cross-shaped junction microchannel. Generally, in a cross-shaped junction microchannel, the continuous phase is injected through two vertical inlets and the dispersed phase through the horizontal inlet (Oishi et al., 2009; Bai et al., 2016, 2018). However, in our studies, the dispersed phase flowed through the vertical inlet and the continuous phase through the horizontal inlet. This distribution is often used in investigations of droplet coalescence (Deng et al., 2013; Arjun et al., 2020). At

the beginning, two interfaces existed when the dispersed phase flowed into the microchannel and interacted with the continuous phase (Fig. 4). With the dispersed phase flowing into the microchannel continuously, the two tips of the dispersed phase became closer to each other. Finally, the two interfaces merged into one. This was followed by the squeezing stage. The dispersed phase blocked the flow of the continuous phase totally, and the continuous phase began to squeeze the dispersed phase. The neck of the dispersed phase became thinner and thinner and finally broke up.

4.2 Quantitative analysis of droplet formation

The characteristics of the droplet, including its length and formation time, are significant parameters for industrial applications. In this section, a quantitative analysis of the droplet length and droplet formation time is presented.

Fig. 5 shows the effect of droplet superficial velocity on droplet length. The dimensionless droplet length is defined as the ratio of droplet length to the microchannel width. Three solid lines represent the average dimensionless droplet lengths in the corresponding dispersed phase fractions. The average dimensionless droplet length $\overline{L_{\text{ave}}}$ is defined as

$$\overline{L_{\text{ave}}} = \frac{\sum \overline{L_{\text{sup}\,i}}}{5}, \tag{8}$$

where $\overline{L_{\text{sup}\,i}}$ represents the dimensionless droplet length at different droplet superficial velocities, i=10, 30, 50, 80, and 100 m/s. In a constant dispersed phase fraction, with the droplet superficial velocity increasing from 10 to 100 mm/s, the droplet length decreased due to the shear force exerted by the continuous phase. However, the changes were within a small range. The droplet length varied within ±15% of the average value. In addition, Fig. 5 indicates that an increase of the dispersed phase fraction led to an increase of the droplet length.

Fig. 6 presents the correlation between the dimensionless droplet formation time and droplet superficial velocity. The dimensionless droplet formation time is determined by the ratio of the droplet formation time to the characteristic time (Christopher et al., 2008). It shows that the dimensionless droplet formation time was reduced with increasing droplet superficial velocity. Meanwhile, as the droplet superficial velocity was

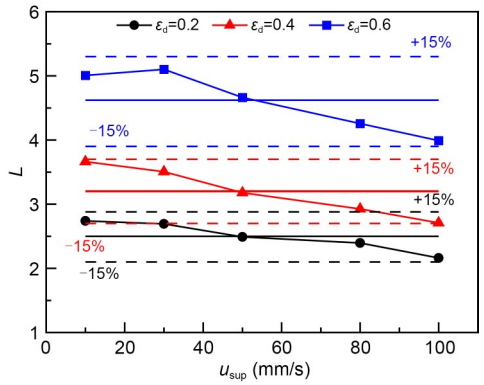

Fig. 5 Variation of the dimensionless droplet length L with different droplet superficial velocities

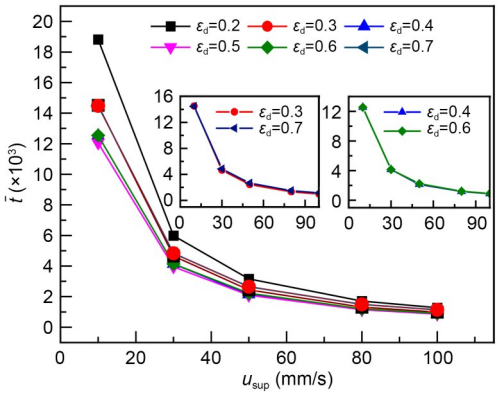

Fig. 6 Variation of dimensionless droplet formation time $\bar{t}$ with different droplet superficial velocities

increased, the effect of the dispersed phase fraction on the droplet formation time decreased. For example, at a constant dispersed phase fraction of 0.5, when the droplet superficial velocity was increased from 10 to 30 mm/s, the dimensionless droplet formation time decreased from 12.05 to 3.95. However, when the droplet superficial velocity was increased from 80 to 100 mm/s, the dimensionless droplet formation time decreased from 1.15 to 0.86. The relative gradients of the droplet formation time were 0.672 and 0.252, respectively. Table 2 lists the detailed values of the relative gradient as the droplet superficial velocity was increased for specific dispersed phase fractions. It also indicates that the relative gradients of the droplet formation time with droplet superficial velocity were independent of the dispersed phase fraction. For example, when the droplet superficial velocity was increased from 30 to 50 mm/s, the relative gradients varied from 0.452 to 0.481 as the dispersed phase fraction changed from 0.2 to 0.7.

Table 2 Relative gradients of droplet formation time with increasing droplet superficial velocity

u_{sup} (mm/s)	Relative gradient of droplet formation time					
	ε_d=0.2	ε_d=0.3	ε_d=0.4	ε_d=0.5	ε_d=0.6	ε_d=0.7
10	–	–	–	–	–	–
30	0.682	0.679	0.670	0.672	0.670	0.666
50	0.472	0.476	0.481	0.471	0.464	0.452
80	0.460	0.460	0.451	0.450	0.516	0.437
100	0.255	0.255	0.260	0.252	0.154	0.240

In addition, Fig. 6 presents the dimensionless droplet formation time for different dispersed phase fractions. At a constant droplet superficial velocity, the droplet formation time changed parabolically with the increase of the dispersed phase fraction. The minimum time for droplet formation was obtained when the dispersed phase fraction was 0.5. Detailed explanations were presented in our previous study (Qian et al., 2019a). Note that since the droplet formation time changed parabolically with the increase of the dispersed phase fraction, the droplet formation time had a similar value when the dispersed phase fractions were 0.4 and 0.6. Also, when the dispersed phase fractions were 0.3 and 0.7, the values were nearly identical. It can be assumed that at a constant droplet superficial velocity, the exchange of the dispersed phase velocity and the continuous phase velocity had a marginal effect on the droplet formation time. However, the exchange of the two-phase velocities had a significant effect on the droplet length. As presented in Fig. 5, the droplet length increased with the increase of the dispersed phase fraction. For example, at a constant droplet superficial velocity of 30 mm/s, the dimensionless droplet length was 3.545 when the dispersed phase fraction was 0.4. When the dispersed phase fraction was 0.6, the dimensionless droplet length increased to 5.123, nearly 1.5 times larger compared to the length measured for 0.4. These findings provide a valuable guide for future operation of droplet formation.

4.3 Inner circulation in the droplet

In micro-scale, due to the shear stress exerted by the wall, a radial velocity gradient exists when non-Newtonian fluids are flowing through a microchannel. The velocity in the axial direction is reduced from the microchannel to the wall. When the droplet is moving through the microchannel, there is not only a velocity gradient in the radial direction due to the shear stress exerted by the wall, but also a velocity gradient in the axial direction due to the interaction with the continuous phase.

Fig. 7a presents the velocity gradient in the droplet radial direction. The x, y directions represent the axial and radial directions of the droplet, respectively. x=0 and y=0 represent the center of the droplet. Several relative positions are marked based on the center of the droplet. When x ranges from −0.325 to 0.225, the velocity gradients in the radial direction are more obvious. In this range, the shear stress exerted by the wall plays an important role in inducing the inner circulation in the droplet. When x>0.225 or x<−0.325, the velocity gradient in the radial direction becomes less obvious. The front and back parts of the droplet are spherical, thus the interaction between the wall and the droplet is weakened. In this range, the shear stress exerted by the continuous phase is dominant.

When the droplet is moving through the microchannel, the front and back parts of the droplet interact with the continuous phase. On the one hand, the

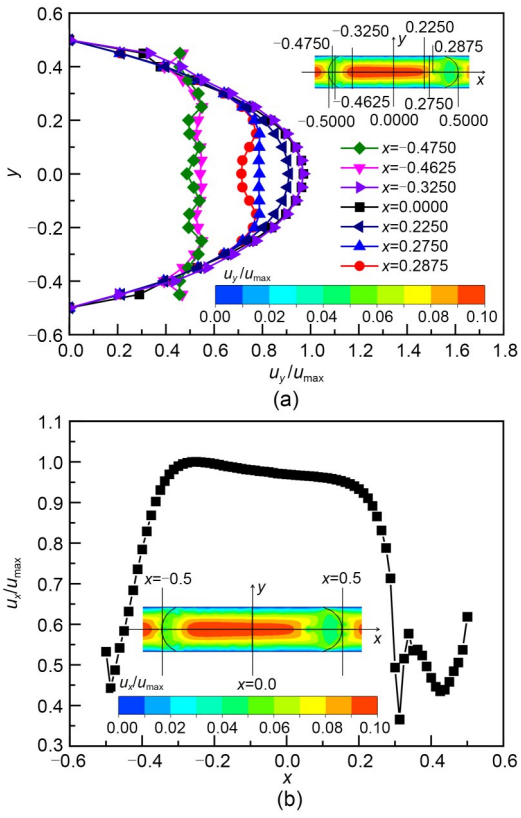

Fig. 7 Velocity gradient in the droplet with u_{sup}=50 mm/s and ε_d=0.5: (a) velocity gradient in the droplet radial direction; (b) velocity gradient in the droplet axial direction

droplet blocks the flow of the continuous phase, which is located upstream of the droplet. On the other hand, the continuous phase, which is located downstream of the droplet, hinders the flow of the droplet. Thus, the interaction of the upstream continuous phase with the back part of the droplet and the interaction of the downstream continuous phase with the front part of the droplet induce the velocity gradient in the droplet axial direction. Fig. 7b presents the velocity gradient in the droplet axial direction. The velocity in the droplet axial direction increases first due to interaction with the upstream continuous phase. Then the velocity in the droplet axial direction decreases slightly since the continuous phase has less effect on the central part of the droplet. Then the velocity in the droplet axial direction decreases greatly due to the interaction with the downstream continuous phase.

As mentioned above, when the droplet is moving through the microchannel, the interactions with the walls and the continuous phase establish velocity gradients in both the radial and axial directions of the droplet. Thus, inner circulation is induced due to the velocity gradients, as shown in Fig. 8. The main circulation is induced by the interaction with the wall, marked as 1. Minor circulation is induced by the interaction with the continuous phase, marked as 2.

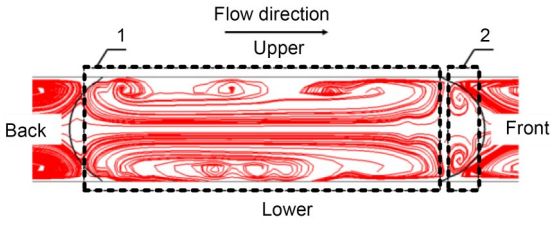

Fig. 8 Schematic diagram of inner circulation in the droplet

4.4 Analysis of mixing efficiency

The mixing efficiency in the droplet can be divided into two stages: the formation stage and the moving stage. The two stages can be visualized by the scalar distribution in the droplet (Fig. 9). At the beginning of the droplet forming stage (Figs. 9a and 9b), scalar redistribution results from the twirling effect induced by the shearing interactions of the continuous phase and dispersed phase. As the droplet grows, the two dispersed phases merge and block the main channel. Subsequently, scalar redistribution is promoted by the interaction with the wall and the continuous phase (Figs. 9c–9f). More importantly, by comparing the conventional distribution of the two (Section 4.1), this initial distribution of the continuous phase and the dispersed phase provides a better platform for subsequent mixing. At the end of the droplet forming stage, the maximum scalar concentration is distributed along the droplet axial direction and decreases gradually from the axis to the wall (Fig. 9d). This kind of distribution is identical to the velocity gradient in the droplet radial direction (Fig. 7a). Considering that the inner circulation in the droplet also occurs symmetrically along the droplet axial direction (Fig. 8), it is evident that as the droplet moves in the microchannel, the mixing process can be strongly facilitated.

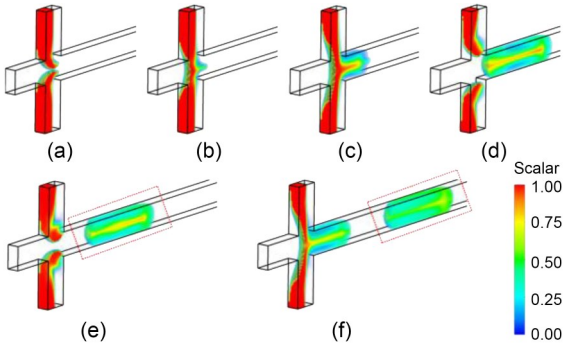

Fig. 9 Scalar distribution in the droplet formation stage and droplet moving stage with u_{sup}=50 mm/s and ε_d=0.5: (a) t=1.0×10^{-3} s; (b) t=2.0×10^{-3} s; (c) t=4.5×10^{-3} s; (d) t=9.5×10^{-3} s; (e) t=12.5×10^{-3} s; (f) t=18.5×10^{-3} s

For a quantitative analysis of the mixing efficiency at different droplet superficial velocities, the scalar concentration of each node in a specified droplet was extracted and compared with the ideal condition. Eq. (5) was selected for quantifying the mixing efficiency.

Fig. 10 presents the variation of the mixing efficiency with the droplet superficial velocity immediately after droplet formation. At a constant dispersed phase fraction, with increasing droplet superficial velocity, the mixing efficiency first decreases and then increases slightly. For example, at a constant dispersed phase fraction of 0.2, with the droplet superficial velocity increasing from 10 to 30 mm/s, the mixing efficiency in the corresponding droplet decreases from 82.8% to 68.2%. However, when the droplet superficial velocity is increased from 80 to 100 mm/s, the mixing efficiency in the corresponding droplet increases from 67.4% to 68.6%.

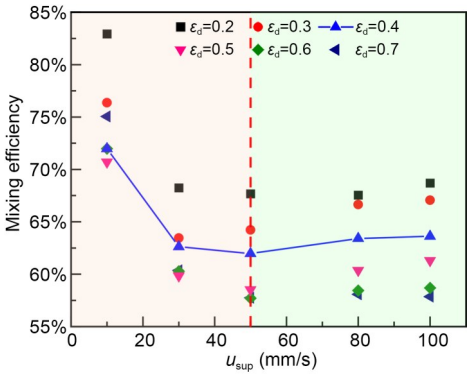

Fig. 10 Mixing efficiency at different droplet superficial velocities at the moment of droplet formation

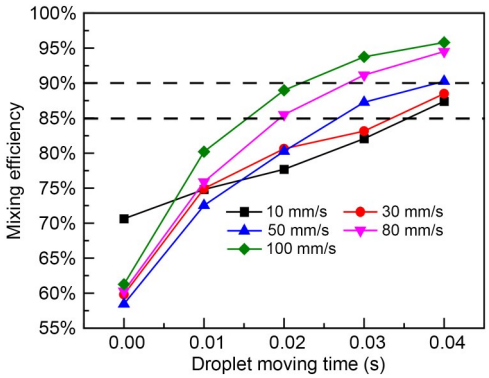

Fig. 11 Mixing efficiency at different droplet superficial velocities in the droplet moving stage with ε_d=0.5

In the droplet formation stage, both droplet length and droplet formation time have significant effects on the mixing efficiency. A longer droplet formation time and a smaller droplet length contribute to a higher mixing efficiency. As discussed in Section 4.2, variation in the droplet superficial velocity affects not only the droplet length, but also the droplet formation time. At a constant dispersed phase fraction, as the droplet superficial velocity increases, the droplet length and droplet formation time both decrease. This presents a reasonable explanation of the effect of the droplet superficial velocity on the mixing efficiency in the droplet. It can be assumed that when the droplet superficial velocity is lower than 50 mm/s, the mixing efficiency in the droplet is time-dominated. Thus, when the droplet superficial velocity increases from 10 to 50 mm/s, the mixing efficiency in the droplet decreases. This is because the droplet formation time is decreased with an increase of the droplet superficial velocity. The time provided for the mixing is reduced. When the droplet superficial velocity is higher than 50 mm/s, the mixing efficiency in the droplet is length-dominated. With the droplet superficial velocity increasing, the droplet length decreases accordingly. The twirling effect is fully induced in the smaller droplet and greatly promotes the mixing efficiency.

At the end of the droplet forming stage as shown in Fig. 9d, the scalar is distributed symmetrically along the axial direction. The scalar concentration decreases from the droplet axial direction to the wall. Thus, during the droplet moving stage, the scalar distribution in the droplet gradually tends to become uniform. The mixing performance is greatly promoted by the inner circulation in the droplet. Fig. 11 shows the mixing efficiency in the droplet moving stage.

In Fig. 11, the time t=0 represents the end of the droplet forming stage. In the droplet moving stage, the droplet length and droplet superficial velocity dominate the mixing efficiency in the droplet. With the increase of the droplet superficial velocity, the droplet length decreases. The circulation path in the droplet is reduced accordingly. The reduced circulation path and the fast circulation time greatly facilitate the mixing efficiency. With the droplet moving in the microchannel, the mixing efficiency gradually increases (Fig. 11). A higher droplet superficial velocity results in a faster mixing process. Importantly, Fig. 11 indicates that at the end of the droplet forming stage, the mixing efficiency is about 60%. After the droplet moves for 0.035 s in the microchannel, the mixing efficiency reaches 85%. This is attributed to the initial distribution of the dispersed phase and the continuous phase. For this arrangement, there is no need for a complex microchannel structure to break the symmetrical inner circulation in the droplet (Özkan and Erdem, 2015; Madadelahi and Shamloo, 2017; Bai et al., 2018; Qian et al., 2019a).

5 Conclusions

In this study, droplet formation and the mixing process in a droplet were investigated via the VOF method coupled with UDS. The effect of droplet superficial velocity on the droplet length, droplet formation time, and mixing efficiency in the droplet were analyzed quantitatively. The conclusions can be summarized as follows:

An increase of the droplet superficial velocity results in a decrease of the droplet length and droplet

formation. As the droplet superficial velocity increases from 10 to 100 mm/s, the droplet length varies within ±15% of the average value. As the droplet superficial velocity increases, the droplet formation time decreases. Also, the effect of the dispersed phase on the droplet formation was investigated. At a constant droplet superficial velocity, the exchange of velocity between the dispersed phase and the continuous phase has a marginal effect on the droplet formation time. However, the operation has a significant effect on the droplet length. These findings provide a valuable guide for the future operation of droplet formation.

Compared with the conventional distribution, the adopted initial distribution of the continuous phase and the dispersed phase provides a better platform for mixing performance. The arrangement causes the scalar concentration to decrease from the droplet axis to the wall, at the end of the droplet forming stage. Thus, the inner circulation in the droplet can be fully utilized. This arrangement also avoids the requirement for a complex structured microchannel. The variation of the droplet superficial velocity influences not only the droplet formation time but also the droplet length. The results indicate that the mixing efficiency in the droplet can be classified into time-dominated and length-dominated regimes. When the droplet superficial velocity is lower than 50 mm/s, the mixing efficiency in the droplet is time-dominated. A longer formation time contributes to a higher mixing efficiency. Thus, the increase in droplet superficial velocity results in a decrease in mixing efficiency. However, when the droplet superficial velocity is higher than 50 mm/s, the mixing efficiency in the droplet is length-dominated. A smaller droplet is more beneficial to the mixing efficiency. Thus, increasing the droplet superficial velocity facilitates the mixing efficiency in the droplet. In the droplet moving stage, the droplet length and droplet superficial velocity dominate the mixing efficiency in the droplet. A higher droplet superficial velocity results in a faster mixing process.

Although the findings highlight the significance of the inner circulation on the mixing process inside the droplet, the distribution of the inner circulation needs to be further addressed. An in-depth study should be carried out in the future to clarify the relationship between the intensity of the inner circulation and the characteristics of the droplet.

Acknowledgments

This work is supported by the National Natural Science Foundation of China (No. 52175067), the Zhejiang Provincial Natural Science Foundation of China (No. LY20E050016), the Key R&D Plan of Zhejiang Province (No. 2021C01021), and the Youth Funds of the State Key Laboratory of Fluid Power and Mechatronic Systems (Zhejiang University) (No. SKLoFP-QN-1801), China.

Author contributions

Jin-yuan QIAN designed the research. Jin-yuan QIAN and Xiao-juan LI processed the data. Jin-yuan QIAN and Lei ZHAO wrote the first draft of the manuscript. Zhi-jiang JIN and Wen-qiang LI helped to organize the manuscript. Lei ZHAO revised and edited the final version.

Conflict of interest

Jin-yuan QIAN, Lei ZHAO, Xiao-juan LI, Wen-qing LI, and Zhi-jiang JIN declare that they have no conflict of interest.

References

Arjun A, Ajith RR, Ranjith SK, 2020. Mixing characterization of binary-coalesced droplets in microchannels using deep neural network. *Biomicrofluidics*, 14(3):034111. https://doi.org/10.1063/5.0008461

Bai L, Zhao SF, Fu YH, et al., 2016. Experimental study of mass transfer in water/ionic liquid microdroplet systems using micro-LIF technique. *Chemical Engineering Journal*, 298:281-290. https://doi.org/10.1016/j.cej.2016.04.034

Bai L, Fu YH, Yao M, et al., 2018. Enhancement of mixing inside ionic liquid droplets through various microchannels design. *Chemical Engineering Journal*, 332:537-547. https://doi.org/10.1016/j.cej.2017.09.086

Borgohain P, Choudhary D, Dalal A, et al., 2018. Numerical investigation of mixing enhancement for multi-species flows in wavy channels. *Chemical Engineering and Processing-Process Intensification*, 127:191-205. https://doi.org/10.1016/j.cep.2018.03.026

Cao YR, Adriaenssens B, de A. Bartolomeu A, et al., 2020. Accelerating sulfonyl fluoride synthesis through electrochemical oxidative coupling of thiols and potassium fluoride in flow. *Journal of Flow Chemistry*, 10(1):191-197. https://doi.org/10.1007/s41981-019-00070-9

Cao Z, Wu Z, Sundén B, 2018. Dimensionless analysis on liquid-liquid flow patterns and scaling law on slug hydrodynamics in cross-junction microchannels. *Chemical Engineering Journal*, 344:604-615. https://doi.org/10.1016/j.cej.2018.03.119

Christopher GF, Noharuddin NN, Taylor JA, et al., 2008. Experimental observations of the squeezing-to-dripping transition in T-shaped microfluidic junctions. *Physical Review E*, 78(3):036317. https://doi.org/10.1103/PhysRevE.78.036317

Dai S, Luo JH, Li J, et al., 2017. Liquid–liquid microextraction

of Cu^{2+} from water using a new circle microchannel device. *Industrial & Engineering Chemistry Research*, 56(44): 12717-12725. https://doi.org/10.1021/acs.iecr.7b01888

Deng NN, Sun SX, Wang W, et al., 2013. A novel surgery-like strategy for droplet coalescence in microchannels. *Lab on a Chip*, 13(18):3653-3657. https://doi.org/10.1039/c3lc50533b

Fu YH, Wang H, Zhang X, et al., 2019. Numerical simulation of liquid mixing inside soft droplets with periodic deformation by a lattice Boltzmann method. *Journal of the Taiwan Institute of Chemical Engineers*, 98:37-44. https://doi.org/10.1016/j.jtice.2018.08.025

Hosseini Kakavandi F, Rahimi M, Jafari O, et al., 2016. Liquid–liquid two-phase mass transfer in T-type micromixers with different junctions and cylindrical pits. *Chemical Engineering and Processing-Process Intensification*, 107:58-67. https://doi.org/10.1016/j.cep.2016.06.011

Jin ZJ, Qiu C, Jiang CH, et al., 2020. Effect of valve core shapes on cavitation flow through a sleeve regulating valve. *Journal of Zhejiang University-SCIENCE A (Applied Physics & Engineering)*, 21(1):1-14. http://doi.org/10.1631/jzus.A1900528

Korczyk PM, van Steijn V, Blonski S, et al., 2019. Accounting for corner flow unifies the understanding of droplet formation in microfluidic channels. *Nature Communications*, 10(1):2528. https://doi.org/10.1038/s41467-019-10505-5

Liu YY, Zhao QK, Yue J, et al., 2021. Effect of mixing on mass transfer characterization in continuous slugs and dispersed droplets in biphasic slug flow microreactors. *Chemical Engineering Journal*, 406:126885. https://doi.org/10.1016/j.cej.2020.126885

Luo XM, Yin HR, Ren J, et al., 2019. Enhanced mixing of binary droplets induced by capillary pressure. *Journal of Colloid and Interface Science*, 545:35-42. https://doi.org/10.1016/j.jcis.2019.03.016

Madadelahi M, Shamloo A, 2017. Droplet-based flows in serpentine microchannels: chemical reactions and secondary flows. *International Journal of Multiphase Flow*, 97: 186-196. https://doi.org/10.1016/j.ijmultiphaseflow.2017.08.010

Mehta V, Rath SN, 2021. 3D printed microfluidic devices: a review focused on four fundamental manufacturing approaches and implications on the field of healthcare. *Bio-Design and Manufacturing*, 4(2):311-343. https://doi.org/10.1007/s42242-020-00112-5

Mu XT, Ju XJ, Zhang L, et al., 2019. Chitosan microcapsule membranes with nanoscale thickness for controlled release of drugs. *Journal of Membrane Science*, 590:117275. https://doi.org/10.1016/j.memsci.2019.117275

Niculescu AG, Chircov C, Birca AC, et al., 2021. Fabrication and applications of microfluidic devices: a review. *International Journal of Molecular Sciences*, 22(4):2011. https://doi.org/10.3390/ijms22042011

Nisisako T, Torii T, Higuchi T, 2004. Novel microreactors for functional polymer beads. *Chemical Engineering Journal*, 101(1-3):23-29. https://doi.org/10.1016/j.cej.2003.11.019

Oishi M, Kinoshita H, Fujii T, et al., 2009. Confocal micro-PIV measurement of droplet formation in a T-shaped microjunction. *Journal of Physics: Conference Series*, 147:012061.

Özkan A, Erdem EY, 2015. Numerical analysis of mixing performance in sinusoidal microchannels based on particle motion in droplets. *Microfluidics and Nanofluidics*, 19(5): 1101-1108. https://doi.org/10.1007/s10404-015-1628-7

Qian JY, Li XJ, Gao ZX, et al., 2019a. Mixing efficiency analysis on droplet formation process in microchannels by numerical methods. *Processes*, 7(1):33. https://doi.org/10.3390/pr7010033

Qian JY, Li XJ, Gao ZX, et al., 2019b. Mixing efficiency and pressure drop analysis of liquid-liquid two phases flow in serpentine microchannels. *Journal of Flow Chemistry*, 9(3):187-197. https://doi.org/10.1007/s41981-019-00040-1

Qian JY, Chen MR, Liu XL, et al., 2019c. A numerical investigation of the flow of nanofluids through a micro Tesla valve. *Journal of Zhejiang University-SCIENCE A (Applied Physics & Engineering)*, 20(1):50-60. http://doi.org/10.1631/jzus.A1800431

Qian JY, Mu J, Hou CW, et al., 2021. A parametric study on unbalanced moment of piston type valve core. *Journal of Zhejiang University-SCIENCE A (Applied Physics & Engineering)*, 22(4):265-276. http://doi.org/10.1631/jzus.A2000582

Sattari-Najafabadi M, Nasr Esfahany M, Wu Z, et al., 2017. Hydrodynamics and mass transfer in liquid-liquid non-circular microchannels: comparison of two aspect ratios and three junction structures. *Chemical Engineering Journal*, 322:328-338. https://doi.org/10.1016/j.cej.2017.04.028

Su YH, Zhao YC, Chen GW, et al., 2010. Liquid-liquid two-phase flow and mass transfer characteristics in packed microchannels. *Chemical Engineering Science*, 65(13): 3947-3956. https://doi.org/10.1016/j.ces.2010.03.034

Tanthapanichakoon W, Aoki N, Matsuyama K, et al., 2006. Design of mixing in microfluidic liquid slugs based on a new dimensionless number for precise reaction and mixing operations. *Chemical Engineering Science*, 61(13): 4220-4232. https://doi.org/10.1016/j.ces.2006.01.047

Tice JD, Song HL, Lyon AD, et al., 2003. Formation of droplets and mixing in multiphase microfluidics at low values of the Reynolds and the capillary numbers. *Langmuir*, 19(22):9127-9133. https://doi.org/10.1021/la030090w

Tsaoulidis D, Angeli P, 2015. Effect of channel size on mass transfer during liquid-liquid plug flow in small scale extractors. *Chemical Engineering Journal*, 262:785-793. https://doi.org/10.1016/j.cej.2014.10.012

Wang JJ, Wang JN, Feng LF, et al., 2015. Fluid mixing in droplet-based microfluidics with a serpentine microchannel. *RSC Advances*, 5(126):104138-104144.

https://doi.org/10.1039/c5ra21181f

Wu JY, Yue Y, Li JY, et al., 2022. Circumferential design of throttling window of main feed water regulating valve and its influence on flow characteristics. *Chinese Journal of Engineering Design*, 29(1):74-81 (in Chinese). https://doi.org/10.3785/j.issn.1006-754X.2022.00.006

Yeh SI, Sheen HJ, Yang JT, 2015. Chemical reaction and mixing inside a coalesced droplet after a head-on collision. *Microfluidics and Nanofluidics*, 18(5-6):1355-1363. https://doi.org/10.1007/s10404-014-1534-4

Zhang J, Xu WH, Xu FY, et al., 2021. Microfluidic droplet formation in co-flow devices fabricated by micro 3D printing. *Journal of Food Engineering*, 290:110212. https://doi.org/10.1016/j.jfoodeng.2020.110212

Zhang PF, Xu XG, Hua YJ, et al., 2022. Effects of the outlet pressure on two-phase slug flow distribution uniformity in a multi-branch microchannel. *Journal of Zhejiang University-SCIENCE A (Applied Physics & Engineering)*, 23(1):68-82. https://doi.org/10.1631/jzus.A2100135

Zhang Q, Liu HC, Zhao SN, et al., 2019. Hydrodynamics and mass transfer characteristics of liquid–liquid slug flow in microchannels: the effects of temperature, fluid properties and channel size. *Chemical Engineering Journal*, 358:794-805. https://doi.org/10.1016/j.cej.2018.10.056

Zhang Y, Zhang XB, Xu BJ, et al., 2015. CFD simulation of mass transfer intensified by chemical reactions in slug flow microchannels. *The Canadian Journal of Chemical Engineering*, 93(12):2307-2314. https://doi.org/10.1002/cjce.22360